

ONBOARD TRAJECTORY OPTIMIZATION FOR RADIUS TO FIX TURNS

Daniel M. Gierszewski¹, Patrick Piprek¹ & Florian Holzapfel¹

¹Institute of Flight System Dynamics, Technische Universität München, 85748 Garching, Germany

Abstract

This paper presents an onboard optimization approach used to generate trajectories for Radius to Fix (RF) turns within an integrated flight guidance and control system. An Optimal Control Problem (OCP) is formulated such that it accounts for the geometric constraints of the RF leg as well as the dynamics and limitations of the closed-loop controlled aircraft. The optimization-based approach overcomes the drawbacks of a geometric trajectory generation method previously published by the authors, which used clothoids for the entry and exit segments of the RF trajectory. Here, the optimization algorithm is functionally decoupled from the safety-critical fight guidance and control modules by means of a Safety Gateway, which verifies the outcome of the optimization algorithm. Optimization as well as verification are performed onboard and online. Besides the OCP formulation, the paper presents details on how the optimization algorithm is embedded into the model-based software design in MATLAB/SimulinkTM to enable deployment on a mission computer. Furthermore, a simulation framework is described that represents the system concept for onboard optimization consisting of the Flight Control Computer (FCC) and the mission computer, which carries out the optimization tasks asynchronously and returns the optimal results via the Safety Gateway to the FCC. This simulation framework is used to illustrate the enhancement of the proposed approach using a flight dynamics model of a CS-23 aircraft.

Keywords: onboard trajectory optimization, onboard trajectory generation, radius to fix, clothoid, waypoint flying

1. Introduction

A Radius to Fix (RF) leg defines a circular track above ground between two waypoints with tangential inbound and outbound legs [1]. The use of RF legs as part of Required Navigation Performance (RNP) operations offers more flexibility in route design and helps to shorten departure and approach procedures, leading to fuel and time savings as well as an increase in airspace capacity [2]. Consequently, automatic flying of waypoint-based flight routes including RF legs is an important functionality in modern flight guidance and control systems for manned and unmanned aerial vehicles. Among other functionality, these systems require an online generation of trajectories for RF turns. Simple approaches combine straight and arc segments to generate the reference trajectory. Using clothoid segments for the entry and exit of the RF turn, as proposed in study [3], results in a linear curvature change and solves the problem of curvature steps at the connection points between straight and arc segments. Trajectory controllers which employ the full nonlinear kinematic error dynamics of second or higher order [4, 5] require sufficiently smooth and feasible trajectories to achieve maximum tracking performance. Clothoids do not meet the required smoothness due to the inevitable kink in curvature resulting in a build-up of horizontal deviations during the transition phases of the RF turn [6, 7]. Moreover, the clothoid approach involves approximations and requires conservative assumptions on the transition time required by the aircraft to build up the bank angle for the RF turn which often results in large differences between the generated trajectory and the originally planned circular RF track [3]. Additionally, the need for conservative assumptions reduces the potential in fuel and time savings.

Thus, this paper proposes the use of trajectory optimization techniques to produce optimal transition trajectories, which consider the actual aircraft dynamics, including the controller. This facilitates the exploitation of the full system dynamics as they require less conservative assumptions in contrast to the purely geometrical approaches. Additionally, the necessary assumptions can be tailored to the specific aircraft and do not require to be generic for different aircraft types. Among others, this solves e.g. the problems of curvature (or higher order derivative) steps as the optimizer can consider a smooth transition by means of constraints. This, in turn, leads to sufficiently smooth feedforward commands that the controlled aircraft is able to follow, improving e.g. the capability of fuel reduction by an improved path following of the controller. For this purpose, also further system constraints can be considered to improve real-world applicability.

The proposed approach is integrated into a trajectory generation function which is part of an automatic flight guidance and control system developed at the authors' institute. This trajectory generation function separates the horizontal and the vertical motion providing the capability of combining vertical autopilot modes, e.g. altitude hold, with horizontal trajectory following.

An important aspect of the incorporation of the onboard optimization in the trajectory generation framework is the separation of the event-based optimization and the time critical flight guidance and control functions. This means that the optimization is conducted while the aircraft is on other geometrical segments (e.g. straight line or arc) and the solution is only used if the calculation is finished in time and provides a meaningful result. The meaningfulness and feasibility of the calculated trajectory is checked by means of a forward simulation before actually providing it to the trajectory generation module ("gateway architecture"). In case this analysis fails, an analytic fallback based on the geometric representation with clothoids of the maneuver is used [3]. The benefit of this approach is that there are no hard real-time requirements on the optimization algorithm as e.g. with model predictive control. This allows the use of general trajectory optimization problem formulations not requiring any simplifications, while being able to utilize the benefits of its onboard applicability.

To detail the proposed methodology, the paper is structured as follows: First, the clothoid-augmented approach is described in Section 2 because it serves as a deterministic fall-back solution in case the optimization does not provide a feasible solution in time. The approach further presents a baseline for comparison. Afterward, the optimization framework and problem formulation are detailed in Section 3. Following, Section 4 provides details about the onboard trajectory generation system and the fallback strategy. Concluding, Section 5 compares the two approaches in simulation, while Section 6 gives conclusive remarks and an outlook.

2. Clothoid-augmented Radius to Fix Trajectory

A RF leg is defined as a constant radius turn between two waypoints as displayed in Figure 1. For the generation of a reference trajectory, clothoid segments are inserted at the beginning and end of the arc to describe the turn entry and turn exit transitions without introducing curvature steps at the connection points between straight line and arc segments. A clothoid is a plane curve \vec{c} , which is described and parameterized by [6] as follows

$$\vec{\mathbf{c}}(\tau) = \begin{bmatrix} x_{cl}(\tau) \\ y_{cl}(\tau) \end{bmatrix} = \begin{bmatrix} A \int_{k=0}^{\tau} \cos(k^2) dk \\ A \int_{k=0}^{\tau} \sin(k^2) dk \end{bmatrix},$$
(1)

where A is the shaping parameter, which specifies the growth rate of the curvature. The running parameter τ determines the length of the clothoid curve and can be interpreted as a dimensionless time. It holds for the arc length s of a clothoid that

$$s(\tau) = A\tau \tag{2}$$

and for the curvature that

$$\kappa_{cl}(\tau) = \frac{2\tau}{A}$$
 (3)

A detailed description on how the clothoid parameters are calculated to construct a clothoid-augmented reference trajectory for a RF leg is given in [3]. Here, only a summary of the approach is given.

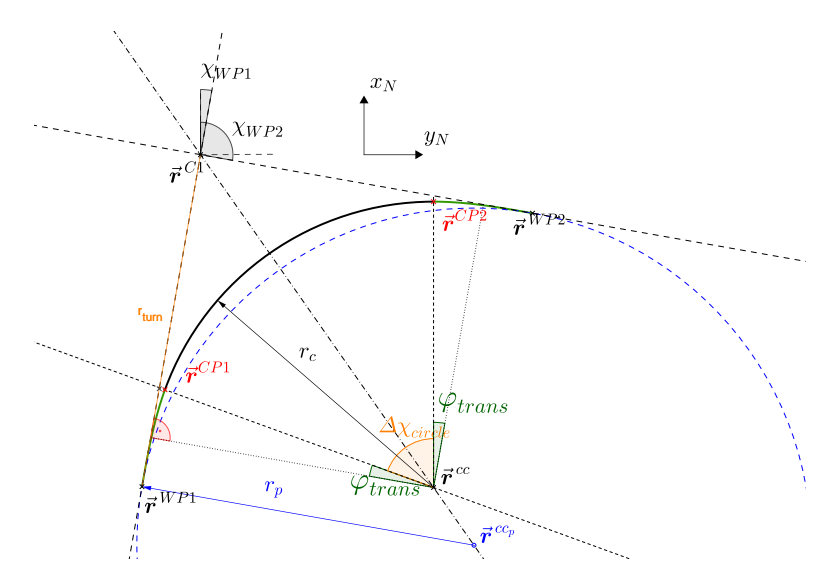


Figure 1 – Radius to Fix maneuver geometry with symmetric turn entry and turn exit transition segments.

First of, a constraint that the curvature at the end of the clothoid matches the curvature of the arc is defined

$$\kappa_{cl}(\tau_{\rm trans}) = \frac{2}{A} \tau_{\rm trans} \equiv \frac{1}{r_c},$$
(4)

where r_c is the circle radius of the RF leg. Assuming a constant speed V_T while flying along the clothoid, the time, t_{trans} , required for the transition maneuver is given by:

$$t_{\text{trans}} = \frac{s_{cl}(0, \tau_{\text{trans}})}{V_T} = \frac{A \tau_{\text{trans}}}{V_T}$$
 (5)

Eliminating the shaping parameter A, by inserting (5) into (4), yields:

$$\tau_{\rm trans}^2 = \frac{V_T t_{\rm trans}}{2r_c} \tag{6}$$

In general, the turn radius r_c can also be determined from the equilibrium of forces of a fixed-wing aircraft flying a turn in a horizontal plane in wind-free condition with zero angle of side-slip and small pitch angle by

$$r_c = \frac{V_T^2}{g\tan(\mu_K)}\,, (7)$$

where μ_K is the kinematic bank angle and g is the gravitational acceleration. Inserting (7) for the radius of the arc segment, r_c , into (6) yields a relationship between τ_{trans} and t_{trans} :

$$\tau_{\text{trans}}^2 = \frac{g}{2V_T} t_{\text{trans}} \tan(\mu_K) \tag{8}$$

The time required for the transition maneuver is defined by the time period it takes the aircraft to reach a certain bank angle. Using the approach of [8], this time period can be approximated by

$$t_{\rm trans} = 2T_p + \frac{\mu}{p_{\rm cmd}},\tag{9}$$

where T_p represents the aircraft roll time constant and $p_{\rm cmd}$ the commanded roll rate. Both parameters are considered as configuration specific design parameters which are determined offline based on the closed-loop roll dynamics of the aircraft. The previous publication [3] proposes to calculate a fixed transient time $t_{\rm trans}^*$ by inserting the maximum allowed bank angle μ_K^* into (9).

However in this study, a different approach was followed which yields improved results. At first, the required bank angle μ_c to maintain a steady-state turn with the circle radius r_p of the RF leg is calculated by

$$\mu_c = \tan^{-1}\left(\frac{V_T^2}{gr_p}\right),\tag{10}$$

where the circle radius r_p of the RF leg is given by the distance of the center fix (CC_P) to the entry or termination fix of the RF leg, here denoted as WP1 and WP2. The positions of the entry and termination fix as well as the circle center are provided by the flight plan. Then, a 2-dimensional look-up table is used to derive an estimate of the transient time $t_{\rm trans}$ as a function of the commanded bank angle μ_c and airspeed. The look-up table data was obtained from non-linear closed-loop simulations of bank angle step commands at different speeds and altitudes. Given (8), the transient parameter $\tau_{\rm trans}$ can be determined by either inserting $t_{\rm trans}^*$ and μ^* when following the approach proposed by [3] or, $t_{\rm trans}$ and μ_c when using the look-up table method.

Once τ_{trans} is determined, the relationships between r_p and r_c that are independent of the shaping parameter A can be derived [3]. With these relationships it is possible to calculate r_c and use (4) to determine A. At this point, the clothoid is fully defined and can be used to derive the geometry of the clothoid-augmented RF trajectory.

Note that the description used in this section is used as a reference to analyze the benefits provided by the optimal transition introduced in Section 3. Additionally, if the optimization is not able to find a valid solution within the given time frame until the segment must be started, the analytic solution provides a secured feasible fallback, which is used to ensure the availablity of a trajectory in the online application as detailed in Section 4.

3. Trajectory Optimization for Radius to Fix Turns

The goal of the optimization is to generate smooth reference trajectories for the transition maneuvers at the entry and exit of the RF turn, thereby replacing the clothoid-augmented approach with an optimal one. Two different Optimal Control Problem (OCP) formulations are used for the turn entry and turn exit: The turn entry is formulated as a constrained trajectory optimization problem, whereas the turn exit is based on a least squares optimization problem of the reversed turn entry segment in order to achieve a turn exit that is symmetric to the turn entry trajectory. This is a valid assumption as the aircraft's performance is similar for rolling in and rolling out. Additionally, this makes it possible to properly compare the optimal solution with the analytic reference introduced in Section 2.

3.1 System Model and Optimal Control Problem for Turn Entry

The system model for the OCP of the turn entry is based on a point-mass model of a fixed-wing aircraft moving in the horizontal plane at a constant height, i.e., with zero climb angle ($\gamma_K=0$). It is further assumed in this study, that the propulsion force points in flight direction, the lateral aerodynamic force is negligible, the absolute kinematic speed V_K is constant throughout the RF turn entry, and no wind is present. These assumptions are only made for the calculation of the optimal RF trajectory, which is the reference path to be followed by the automatic path control described in Section 3.3. The path control loop compensates for deviations caused by wind and speed changes which can occur while executing the maneuver. The position is propagated in the locally fixed, two-dimensional Ti-frame. Its origin is in ($\vec{\mathbf{r}}^{WP1}$) and the orientation is derived by rotating the North-East-Down (O) frame by the course angle χ_{Ti} about the z_O -axis such that the x_{Ti} -axis points along the tangent of the circular arc of the RF leg (see Figure 1):

$$\begin{bmatrix} \dot{x} \\ \dot{y} \end{bmatrix}_{T_i}^E = \begin{bmatrix} V_K \cos(\chi_K - \chi_{T_i}) \\ V_K \sin(\chi_K - \chi_{T_i}) \end{bmatrix}_{T_i}^E$$
(11)

When considering the turn entry segment χ_{Ti} is equal to the course angle χ_{WP1} of the inbound leg. The aircraft course angle is given by χ_K . The translational equation of motion in the horizontal plane is described in the kinematic frame K assuming a non-rotating, flat earth, constant gravity, and no mass change as follows:

$$\dot{\chi}_K = \frac{g}{V_K} \tan(\mu_K) \tag{12}$$

The actual, closed-loop roll dynamics of the aircraft are incorporated into the optimization by using a linear transfer function model of fourth order:

$$G_{\mu_K \mu_{K,\text{cmd}}}(s) = \frac{b_3 s^3 + b_2 s^2 + b_1 s + b_0}{s^4 + a_3 s^3 + a_2 s^2 + a_1 s + a_0},$$
(13)

where a_i with $i = \{0,1,2,3\}$ are the denominator and b_j with $j = \{0,1,2,3\}$ are the numerator coefficients. A maximum order of four was considered as sufficient for an accurate approximation of the nonlinear closed loop roll dynamic.

To use the transfer function in (13) within trajectory optimization, a specification in the observable canonical form is beneficial [9]:

$$\dot{\mathbf{x}}_{\mu} = \begin{bmatrix} 0 & 0 & 0 & -a_0 \\ 1 & 0 & 0 & -a_1 \\ 0 & 1 & 0 & -a_2 \\ 0 & 0 & 1 & -a_3 \end{bmatrix} \mathbf{x}_{\mu} + \begin{bmatrix} b_0 \\ b_1 \\ b_2 \\ b_3 \end{bmatrix} u_{\mu}$$

$$y_{\mu} = \begin{bmatrix} 0 & 0 & 0 & 1 \end{bmatrix} \mathbf{x}_{\mu}$$
(14)

Within this formulation, it is $u_{\mu} = \mu_{K, \mathrm{cmd}}$ while $y_{\mu} = \mu_{K}$, and consequently the evaluation with known quantities is straightforward, which also eases the bounding by means of constraints in optimization. The coefficients are determined by estimating a fourth-order transfer function model using the *System Identification Toolbox* from Mathworks[®]. For the simulation results of this paper, the estimation was performed using frequency-domain data that was obtained from the nonlinear closed-loop simulation model at varying static and dynamic pressures. In contrast, for the real-world application, the transfer function coefficients are determined using frequency-domain data that were obtained during flight tests for gain tuning of the lateral inner-loop controller [10, 11]. It should be noted that the coefficients are retrieved from tabulated values in the beginning of the optimization (based on the planned speed and dynamic pressure of the maneuver) and then kept constant within the optimization. This is a valid assumption as both speed and altitude should not change drastically during the maneuver.

The state vector and control variable of the system model for the optimization are consequently given by:

$$\mathbf{x} = \begin{bmatrix} x_{Ti} & y_{Ti} & \chi_K & \mu_K & \dot{\mu}_K & \ddot{\mu}_K & \ddot{\mu}_K & \mu_{K,\text{cmd}} & \dot{\mu}_{K,\text{cmd}} \end{bmatrix}^\mathsf{T}$$
 (15)

$$u = \ddot{\mu}_{K \text{ cmd}} \tag{16}$$

It is worth noting here that the commanded bank angle $\mu_{K,\mathrm{cmd}}$ is not a direct command into the system but rather its second time derivative $\ddot{\mu}_{K,\mathrm{cmd}}$, which is integrated twice to obtain the commanded bank angle. This is done to smoothen the optimal control input and avoid bank angle step commands, which are unphysical. Furthermore, the states μ_K , $\dot{\mu}_K$, $\ddot{\mu}_K$, and $\ddot{\mu}_K$ represent the dynamics prescribed by (14).

The OCP is minimizing $(y_{Ti})^2$, i.e., the squared deviation from the straight line during the turn entry. This results in a timely conduction of the maneuver and is formulated as:

$$J = \int_{t=0}^{t_{\text{trans}}} (y_{Ti}(t))^2 dt$$
 (17)

Path constraints are defined for the load factor and to enforce the geometric constraints of the RF turn. The body-frame load factor in z_B direction during a turn with constant speed and altitude is given by:

$$n_{z,B} = \frac{1}{g}\sin(\mu_K)\cos(\alpha_K)V_K\dot{\chi}_K + \cos(\alpha_K)\cos(\mu_K)$$
(18)

The angle of attack α_K for straight and level trim condition is used in the evaluation of this equation. Note that the constraint in (18) is required to not overstress the aircraft.

Furthermore, the following constraint is used to enforce a complete transition onto the arc during the optimization:

$$\frac{V_T}{\dot{\chi}(t_{\rm trans})} - r_c \equiv 0 \tag{19}$$

The exact mathematical formulation of this constraint is dependent on the turn angle $\Delta \chi = \chi_{WP2} - \chi_{WP1}$ (mapped to the interval $[-180^{\circ}; 180^{\circ}]$; as indicated in Figure 1), which results in the radius of the arc r_c . The following three cases describe the different specifications:

1.
$$\Delta \chi < 180^{\circ}$$

$$r_c = \frac{\sin(\frac{\pi - \Delta \chi}{2})}{\sin(\frac{\Delta \chi}{2} - \Delta \chi(t_{\text{trans}}))} \left(r_{\text{turn}} - \frac{|\Delta y(t_{\text{trans}})|}{\tan(\frac{\pi}{2} - \Delta \chi(t_{\text{trans}}))} - |\Delta x(t_{\text{trans}})| \right)$$
(20)

2.
$$\Delta \chi = 180^{\circ}$$

$$r_c = \frac{1}{\cos(\Delta \chi(t_{\text{trans}}))} \left(\frac{\|\vec{\mathbf{r}}^{WP_1WP_2}\|}{2} - |\Delta y(t_{\text{trans}})| \right)$$
 (21)

3. $\Delta \chi > 180^{\circ}$

$$r_{c} = \sin\left(\frac{\Delta\chi(t_{\text{trans}}) - \pi}{2}\right) \left(\frac{r_{\text{turn}} + |\Delta\chi(t_{\text{trans}})| + \frac{|\Delta y(t_{\text{trans}})|}{\cot(\Delta\chi(t_{\text{trans}}))}}{\cos(\frac{\Delta\chi - \pi}{2} - \Delta\chi(t_{\text{trans}}))}\right) - \frac{|\Delta y(t_{\text{trans}})|}{\cos(\Delta\chi(t_{\text{trans}}))}$$
(22)

where r_{turn} denotes the distance between $\vec{\mathbf{r}}^{WP_1}$ and the intersection of the tangents $\vec{\mathbf{r}}^{C1}$ as shown in Figure 1. It should finally be noted that the transfer function model in (14) is enforced to be in steady state (i.e. $\dot{\mathbf{x}}_{\mu} = \mathbf{0}$) at the initial and final point of the optimization to ensure a smooth transition. Based on the previous specifications, the following OCP is defined:

$$\begin{aligned} & \underset{u(t)}{\min} & \text{ (17)} \\ & \text{ s.t. } & \mathbf{x}_{lb} \leq \mathbf{x} \leq \mathbf{x}_{ub} \\ & \mathbf{x}_{IBC,lb} \leq \mathbf{x}(t_0) \leq \mathbf{x}_{IBC,ub} \text{ ((28) and (29))} \\ & \mathbf{x}_{FBC,lb} \leq \mathbf{x}(t_f) \leq \mathbf{x}_{FBC,ub} \text{ ((30) and (31))} \\ & u_{lb} \leq u \leq u_{ub} \\ & \dot{\mathbf{x}}_{\mu}(t_0) = \mathbf{0} \\ & \dot{\mathbf{x}}_{\mu}(t_f) = \mathbf{0} \\ & \text{ (18)} \\ & \text{ (19) (with (20) - (22))} \end{aligned}$$

The optimization variable bounds are defined as follows:

$$\mathbf{x}_{lb} = \begin{bmatrix} -\infty & -\infty & -\infty & -45^{\circ} & -\infty & -\infty & -45^{\circ} & -20^{\circ}/s \end{bmatrix}^{\mathsf{T}} \tag{24}$$

$$\mathbf{x}_{\mathrm{ub}} = \begin{bmatrix} +\infty & +\infty & +\infty & +45^{\circ} & +\infty & +\infty & +45^{\circ} & +20^{\circ}/\mathrm{s} \end{bmatrix}^{\mathsf{T}} \tag{25}$$

$$u_{\rm lb} = -8^{\circ}/{\rm s}^2$$
 (26)

$$u_{\rm ub} = +8^{\circ}/\mathrm{s}^2 \tag{27}$$

Note that the states within the observable canonical form (see (14)) generally do not need to be bounded as the output as well as the command control chain will ensure a sensible state history. It should be noted that the bounds in (24) and (25) are the general lower and upper bounds for the state variables. At the initial and final time, the following bounds are defined:

$$\mathbf{x}_{\text{IBC,lb}} = \begin{bmatrix} 0 & 0 & 0^{\circ} & 0^{\circ} & 0^{\circ}/s & 0^{\circ}/s^{2} & 0^{\circ}/s^{3} & 0^{\circ} & 0^{\circ}/s \end{bmatrix}^{\mathsf{T}}$$
 (28)

$$\mathbf{x}_{\text{IBC,ub}} = \begin{bmatrix} 0 & 0 & 0^{\circ} & 0^{\circ} & 0^{\circ} / s & 0^{\circ} / s^{2} & 0^{\circ} / s^{3} & 0^{\circ} & 0^{\circ} / s \end{bmatrix}^{\mathsf{T}}$$
(29)

$$\mathbf{x}_{\text{FBC},\text{lb}} = \begin{bmatrix} 0 & 0 & 0^{\circ} & -45^{\circ} & -\infty & -\infty & -\infty & -45^{\circ} & 0^{\circ}/\text{s} \end{bmatrix}^{\mathsf{T}}$$
(30)

$$\mathbf{x}_{\text{FBC},\text{ub}} = \begin{bmatrix} +\infty & +\infty & +45^{\circ} & +45^{\circ} & +\infty & +\infty & +\infty & +45^{\circ} & 0^{\circ}/\text{s} \end{bmatrix}^{\mathsf{T}} \tag{31}$$

Take into account that setting the positions and course angle to 0 is without loss of generality as all RF turns can be transformed such that they start in this condition. The offsets occurring from this must then be added to the obtained optimal solution.

The OCP in (23) is transformed using a direct trapezoidal discretization method as implemented in FALCON.m [12]. The resulting nonlinear program is solved using IPOPT [13] with the ma97 solver [14]. The initial guess is based on a linear interpolation between the guess of the expected initial and final states. Such a guess may be obtained by evaluating the analytic equations provided by the clothoid in Section 2 (if no guess is available the mean of lower and upper bound defined in (24) and (25) may be used). The feasibility and optimality tolerance are set to 10^{-5} . The resulting OCP is coded in C++ such that it can be used onboard the aircraft as well as within the simulation environment.

3.2 System Model and Optimal Control Problem for Turn Exit

For the exit of the RF, a symmetry of the position is assumed. However, as the commands may be different an additional OCP must be solved. The state vector (including bounds) and control variable of this second problem are given as follows:

$$\hat{\mathbf{x}} = \begin{bmatrix} \chi_K & \mu_K & \dot{\mu}_K & \ddot{\mu}_K & \ddot{\mu}_K & \mu_{K,\text{cmd}} & \dot{\mu}_{K,\text{cmd}} & \hat{t} \end{bmatrix}^\mathsf{T}$$
(32)

$$\hat{u} = \ddot{\mu}_{K, \text{cmd}} \tag{33}$$

$$\hat{\mathbf{x}}_{lb} = \begin{bmatrix} -\infty & -45^{\circ} & -\infty & -\infty & -\infty & -45^{\circ} & -20^{\circ}/s & 0 \end{bmatrix}^{\mathsf{T}} \tag{34}$$

$$\hat{\mathbf{x}}_{ub} = \begin{bmatrix} +\infty & +45^{\circ} & +\infty & +\infty & +\infty & +45^{\circ} & +20^{\circ}/s & +\infty \end{bmatrix}^{\mathsf{T}}$$
(35)

$$\hat{\mathbf{x}}_{\text{IBC,lb}} = \begin{bmatrix} -(1+\varepsilon)\chi_{\text{des}}(t_f) & 0^{\circ} & 0^{\circ}/\text{s} & 0^{\circ}/\text{s}^{2} & 0^{\circ}/\text{s}^{3} & -45^{\circ} & 0^{\circ}/\text{s} & 0\text{s} \end{bmatrix}^{\mathsf{T}}$$
(36)

$$\hat{\mathbf{x}}_{\text{IBC,ub}} = \begin{bmatrix} -(1-\varepsilon)\chi_{\text{des}}(t_f) & 0^{\circ} & 0^{\circ}/\text{s} & 0^{\circ}/\text{s}^{2} & 0^{\circ}/\text{s}^{3} & +45^{\circ} & 0^{\circ}/\text{s} & 0\text{s} \end{bmatrix}^{\mathsf{T}}$$
(37)

$$\hat{\mathbf{x}}_{\text{FBC,lb}} = \begin{bmatrix} 0^{\circ} & -(1+\varepsilon)\mu_c & -\infty & -\infty & -\infty & -45^{\circ} & 0^{\circ}/\text{s} & t_f \end{bmatrix}^{\mathsf{T}}$$
(38)

$$\hat{\mathbf{x}}_{\text{FBC,ub}} = \begin{bmatrix} 0^{\circ} & -(1-\varepsilon)\mu_c & +\infty & +\infty & +\infty & +45^{\circ} & 0^{\circ}/\text{s} & t_f \end{bmatrix}^{\mathsf{T}}$$
(39)

Thus, the horizontal positions are removed from the OCP, while the time \hat{t} is explicitly added. Note that the positions can be removed as they are directly dependent on the course angle due to the constant speed (see (11)). Thus, tracking the two positions is reduced to tracking the course angle, consequently reducing the problem complexity. It should furthermore be noted that $\chi_{\rm des}$, i.e. the desired course angle that is to be covered by the transition, can be obtained once the OCP in (23) is solved. Additionally, it may be calculated by evaluating the polynomial fit in (41). This assignment is done in that way due to the symmetry requirement introduced in Section 2 and Figure 1.

Further take into account that the transfer functions for turn entry and turn exit may not be the same and thus, following the same trajectory requires different control inputs and consequently a dedicated optimization. Additionally, most often transfer functions are not calculated in banked flight, but only for wings-level motion. This is also the case for here, requiring the final limitation of the physical bank angle to μ_c , which is calculated by (10) to represent the bank angle as required for flying the arc. Due to the specification of the transfer function, the conditions in (36)–(39) start from "wings-level" flight. However, this bank angle state is only internal to ensure that the transfer function is evaluated starting from wings-level. For the physical state evaluation, as e.g. in (12), the bank angle of the arc μ_c is added. Therefore, the bank angle states in (32) as well as the command in (33) should be understood as deviations from the trim state, which is the bank angle required to fly the arc.

Finally, in order to improve the convergence of the OCP, the bounds for the course angle at the initial condition and the bank angle at the final condition in (36)–(39) are softened by introducing the slack parameter ε . For the results presented in this paper, this parameter was set to $\varepsilon=0.1$. This is viable as the trajectory controller will reduce any deviations that may result from this. Additionally, the differences should only be small as the optimizer will try to follow the course angle from the turn entry as defined in (42).

The cost function for the exit problem is consequently designed to track the course angle of the turn entry maneuver as follows:

$$\hat{J} = \int_{t=0}^{\hat{t}_f} (\chi_K - \chi_{\text{des}})^2 dt$$
 (40)

Here, the variable χ_{des} indicates the desired evolution of the course angle which is obtained by a polynomial least squares fit of order n (in the application scenarios, n=7 proved to be sufficiently accurate) for the turn entry trajectory obtained from (23). The variable χ_{des} is then calculated by:

$$\chi_{\text{des}}(\hat{t}) = -\sum_{k=0}^{n} p_k \cdot (t_f - \hat{t})^k \tag{41}$$

The two important aspects of (41) are that the coefficients obtained from the turn entry are multiplied by -1 and that the time is evaluated based on the optimal final time result obtained from the OCP in (23). These adaptations are based on the fact that the exit trajectory is started in a banked condition and turns out to wings-level flight, which is exactly the opposite behavior to the turn entry. Thus, the polynomial must also be evaluated in the "opposite" manner.

Based on the previous specifications, the following OCP has to be solved for the turn exit:

This problem is again solved using IPOPT with the same optimality and feasibility tolerances as described in Section 3.1 for the turn entry.

3.3 Command Generation for Automatic Path Control

For the command generation to the path controller, the OCP solution obtained from (23) and (42) is approximated by a polynomial fit. This is done to ensure that the footpoint required for the trajectory controller can be calculated with available methods [6, 15]. Additionally, the comparability to the clothoid-based approach is ensured by this. This polynomial regression model can be expressed in matrix form as follows:

$$\begin{bmatrix} y_1 \\ \vdots \\ y_n \end{bmatrix} = \begin{bmatrix} 1 & x_1 & x_1^2 & \cdots & x_1^m \\ \vdots & \vdots & & \vdots \\ 1 & x_n & x_n^2 & \cdots & x_n^m \end{bmatrix} \begin{bmatrix} a_0 \\ \vdots \\ a_m \end{bmatrix} + \begin{bmatrix} \varepsilon_1 \\ \vdots \\ \varepsilon_n \end{bmatrix}$$

$$(43)$$

which can be written in pure matrix notation as:

$$\vec{\mathbf{y}} = \mathbf{X}\vec{a} + \vec{\varepsilon} \tag{44}$$

where the response vector \vec{y} corresponds to the optimal time histories for x_{Ti} , y_{Ti} and $\mu_{K,\text{cmd}}$ for the turn entry or turn exit. The variables x_i refer to the time grid of the discretized OCP.

Using least squares regression, an estimation for the polynomial coefficients can be derived as follows:

$$\widehat{\vec{a}} = (\mathbf{X}^{\mathsf{T}}\mathbf{X})^{-1}\mathbf{X}^{\mathsf{T}}\vec{y} \tag{45}$$

Here, m < n is required for invertibility. Additionally, invertibility is guaranteed if all x_i are distinct values. As this is the case for the OCP formulations defined by (23) and (42), the polynomial coefficients can be calculated and the generated optimal trajectories can be deployed in the available trajectory generation module [6, 15].

4. Onboard Application

The proposed onboard trajectory optimization approach has been developed as part of a research project [16] for which a CS-23 [17] class Grob G-520T single engine turboprop aircraft was modified to serve as an Optionally Piloted Vehicle (OPV) demonstrator. Typical use cases for this aircraft are surveillance and observation missions, often including a significant number of RF turns, e.g., for search patterns. Achieving a high trajectory tracking performance for automatic trajectory flying of RF turns is therefore of particular interest for this application as it reduces the fuel consumption and thus increases the exploration radius. A digital flight control system was installed on the aircraft with a Flight Control Computer (FCC) and electro-mechanical actuators that can be decoupled from the normal mechanical controls via safety clutches [18]. The FCC accommodates the flight guidance and control software that was developed at the authors' institute for OPV applications [15]. The algorithms were already successfully tested in flight with several aircraft types like a DA42 M-NG [15], a Dornier DO 282-101, and the very-light electric aircraft "ELIAS" [19]. Ethernet interfaces of the installed FCC can be used for a connection to a separate Mission Computer, which is required for the proposed system concept.

4.1 System Concept

The system concept for onboard trajectory optimization was introduced in a previous publication [20] for the onboard generation of fuel-optimal climb trajectories. A key aspect of the proposed system concept is the separation of the event-based, computational intensive trajectory optimization functionality from the safety critical flight guidance and control functionalities that need to meet hard real-time requirements.

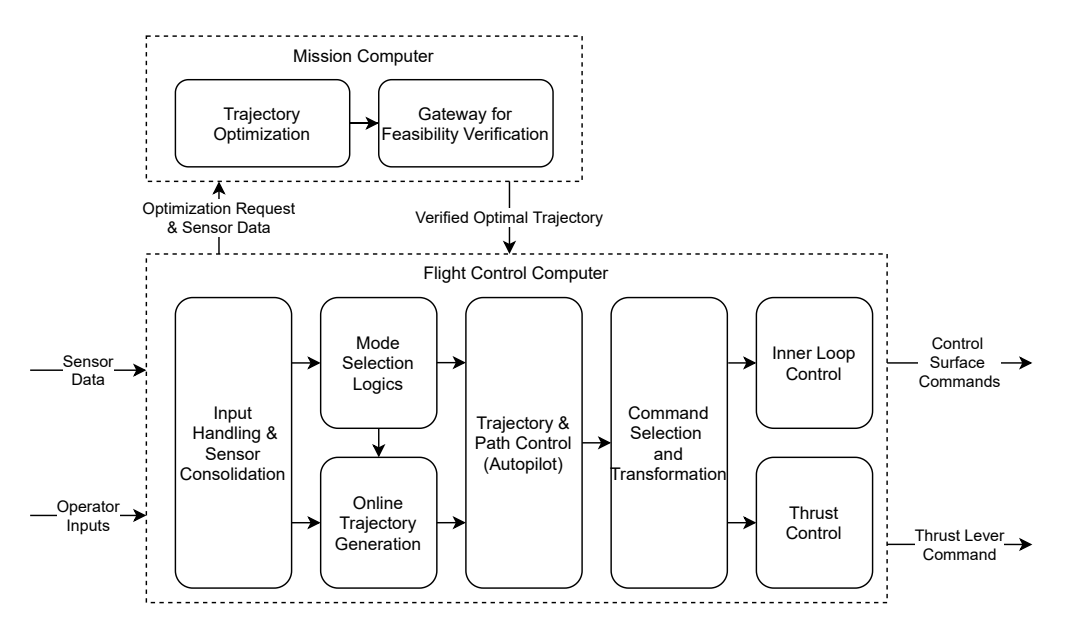


Figure 2 – Functional modules for online trajectory optimization and automatic flight control (taken from [20]).

Figure 2 illustrates the system concept and the allocation of functions to the two computers: A FCC accommodating the time-critical flight guidance and control software and a mission computer, which provides the required computational power to execute the optimization algorithm. The optimization results are verified by a *Gateway* function before being sent to the FCC for deployment. The *Gateway* function was introduced in [20] for onboard trajectory optimization and in [21] for offline use. The optimization is triggered either manually by the operator in case of active autopilot operation, e.g., to start a fuel-optimal climb, or automatically by the Trajectory Generation (TrajGen) function in case of active waypoint-based lateral and/or vertical navigation. For more information on the use of the TrajGen function for automatic flight guidance the reader is referred to [22].

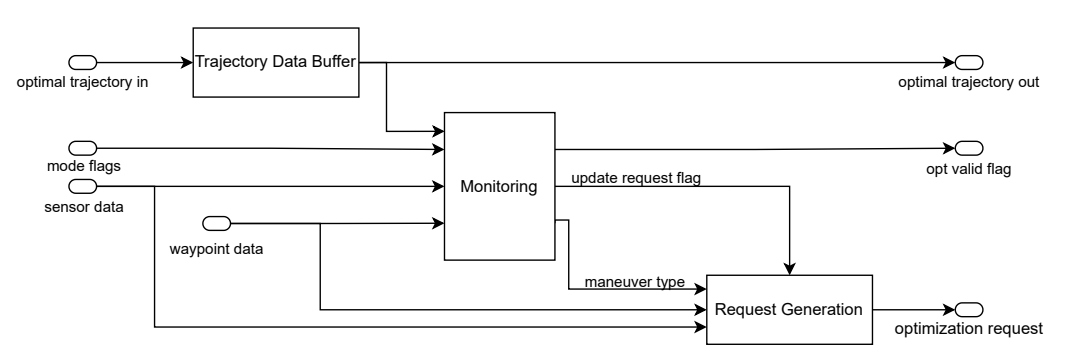


Figure 3 – Interface modules for online trajectory optimization.

The software that implements the TrajGen function is extended by an additional interface module to support onboard trajectory optimization. Figure 3 provides a simplified representation of the interface module as implemented in Simulink. The *Monitoring* subsystem uses the incoming *waypoint data* of the active flight plan to detect if a maneuver is imminent for which the trajectory optimization can be used. The *waypoint data* contains the subset of waypoints from the active flight plan, which is directly used for the generation of flight path commands: FROM (where the aircraft comes from), TO (where the aircraft is currently proceeding to), and NEXT (where the aircraft will proceed to after reaching the TO). Each waypoint consists of a data set including waypoint position and leg type information according to the ARINC 424 standard [23]. If a NEXT waypoint with a RF as leg type is detected by the *Monitoring* subsystem, the *Request Generation* subsystem is enabled to output an *optimization request* that is sent from the FCC to the mission computer.

This *optimization request* is a Simulink[™] bus structure containing the following data in case the optimization is to be applied for a RF maneuver:

- Identification number for optimization request (Request ID)
- · Static pressure
- Indicated airspeed
- Identifier for horizontal or vertical maneuver types (maneuver_type_index)
- Absolute kinematic velocity (V_K^R)
- Turn distance (r_{turn})
- Change in course angle during RF turn ($|\Delta \chi_{abs}|$)

The turn distance r_{turn} was introduced in Section 3.1 as the distance between WP1 and the intersection point of the tangents. In case the intersection does not exist as the tangents are parallel, i.e. $\Delta \chi = 180^{\circ}$, r_{turn} is defined as the horizontal distance between the initial and ending fix of the RF leg, in Figure 1 denoted as as WP1 and WP2.

The *Trajectory Optimization* module on the mission computer recognizes a newly received *optimization request* by a change in the *Request ID*. Whenever the *Request ID* changes, any ongoing execution of an optimization algorithm is stopped and a new run is initiated for the maneuver that is specified by the *maneuver_type_index*.

Once the algorithm has been executed and an optimal solution has been found, the Trajectory Optimization forwards the results to the Gateway for a feasibility check before sending the results together with the request Request ID back to the FCC. After sending a request, the Monitoring on the FCC awaits new optimization results data (optimal trajectory in) containing a Request ID that is identical to that of the sent request. The identification number Request ID is hereby used to check if the received optimization results are still valid and ready for use. The Monitoring subsystem constantly monitors the parameters that are used as inputs and/or constraints for the optimization and a new request with a new Request ID is issued if a change to any of the parameters exceeds a permissible threshold value. This allows to re-run the optimization with the latest information on wind, speed, etc. as long as the maneuver, which is related to the optimization results, has not yet been started. Additionally, it ensures that an optimal solution that is no longer adequate for the present conditions is not processed. Incoming results for an optimal trajectory are stored by the Trajectory Data Buffer subsystem as long as the Request ID included in the received data matches the last generated request Request ID. As soon as the aircraft reaches the TO waypoint which marks the entry of the RF turn, and Monitoring outputs a positive opt valid flag, the optimal trajectory data is forwarded to the TrajGen function to generate a reference path and trajectory control commands. The opt valid flag indicates that the optimal flight guidance is enabled by the user and that current as well as verified optimal trajectory data are available. If the opt valid flag is False at the moment when the aircraft reaches the entry of the RF turn, the TrajGen function uses the standard clothoid-based approach (see Section 2) to generate a reference path and trajectory control commands.

4.2 Software Development of the Trajectory Optimization Function

A model-based design workflow using SimulinkTM and StateflowTM is implemented for the software development of the *Trajectory Optimization* function. A hybrid design approach, which is based on the work by [24], is used for the implementation. Figure 4 illustrates the SimulinkTM implementation of the subsystem generating the entry and exit turn trajectory segments of the RF turn using trajectory optimization. This subsystem includes functions implemented in SimulinkTM and S-functions to incorporate the C++ code of the optimization algorithms into the SimulinkTM model.

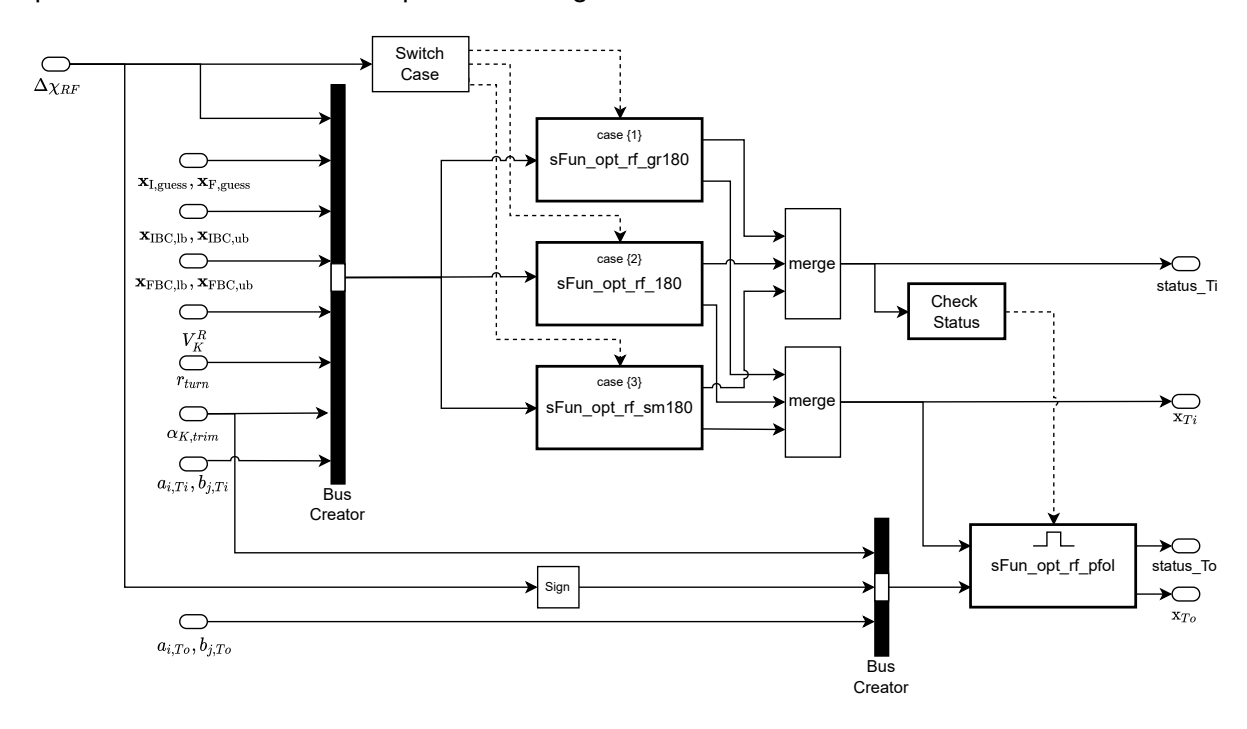


Figure 4 – Simplified hybrid architecture of Trajectory Optimization software with S-functions.

For these systems, the parameters specifying the desired execution of the RF maneuver uniquely (such as the turn radius r_{turn} , speed V_K^R , transfer function coefficients for turn entry $a_{i,Ti}$, $b_{i,Ti}$ and for turn exit $a_{i,To}$, $b_{i,To}$, etc., see Section 3) can be specified from the outside. By this, the same code can be re-used for multiple different problem statements, therefore allowing for general applicability of the

code. The Legacy Code ToolTM is used for the integration of the external C++ code into the SimulinkTM model for validation and verification using Model-in-the-Loop (MIL) simulation. When code is generated, the legacy C++ code files are identified and a function call is inserted into the generated code. The external C++ code includes third-party libraries, such as IPOPT [13], which are not formally developed under DO-178C. The optimization function is therefore considered as unsafe and consequently decoupled from the safety-critical software part of the flight guidance and control software by means of the *Gateway for Feasibility Verification*.

5. Simulation Results

The proposed methodology of Sections 3 and 4 is displayed in the following through simulation results obtained from a high-fidelity CS-23 MIL simulation environment.

5.1 Model-in-the-Loop Simulation Environment

A MIL simulation environment has been developed to design and test the proposed onboard trajectory optimization system in Simulink[™]. The MIL contains a closed-loop simulation model of the G-520T, which was developed based on the work by [25] for the design and verification of the FCC software as part of different research projects [16, 18].

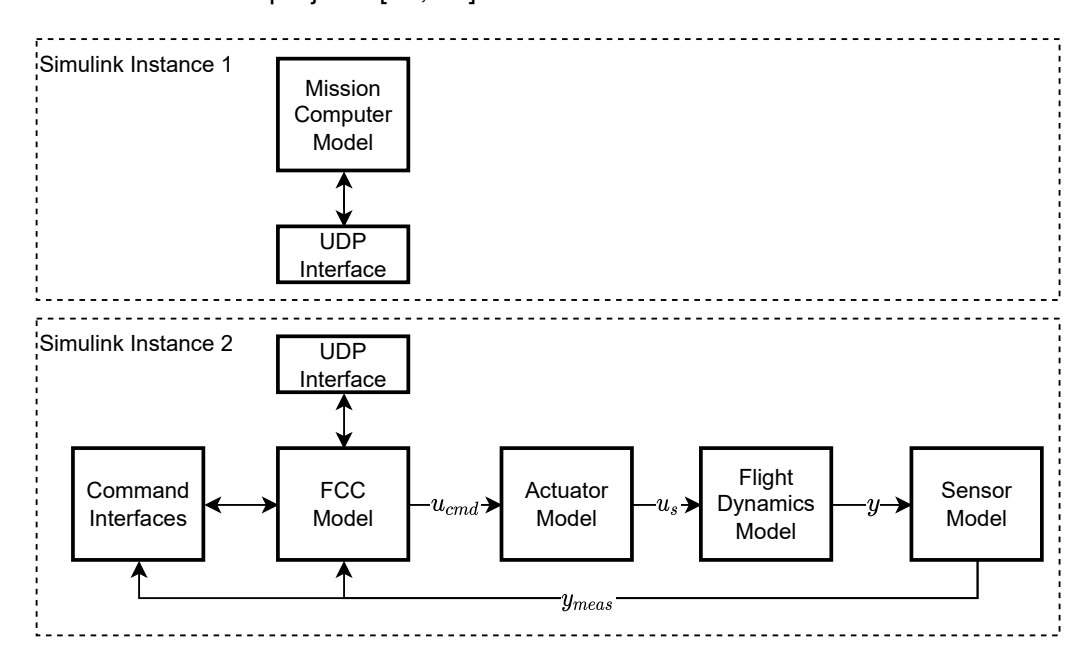


Figure 5 – Overview of MIL simulation (Instance 2 part with FCC is adopted from [25]).

As illustrated in the lower part of Figure 5 the closed-loop model includes the rigid-body flight dynamics model of the G-520T, actuator dynamics, sensor models, and a model of the FCC with the flight guidance and control software. Virtual versions of a Mode Control Panel (MCP) and a Monitoring Display are used as command interfaces, which exchange data with the FCC model for controlling and monitoring the automatic flight modes. In real application, physical versions of the MCP and Monitoring Displays are integrated into the cockpit of the G-520T and additionally used on the ground station for remote control and monitoring of the aircraft via a data-link connection. Instead of manual user inputs, pre-defined MCP inputs were fed into the FCC model to derive the simulation results shown in this paper. Upon the start of a simulation run, pre-defined MCP inputs are used to engage the auto-thrust function for airspeed control and to activate waypoint-based lateral and vertical navigation modes for automatic path-following control. For obtaining the simulation results presented in this paper, waypoints of an exemplary flight plan that includes two different RF legs were loaded to the FCC. While the FCC is executed as a discrete-time model with a sample rate of 100 Hz, continuous-time domain modeling is used for the actuator and flight dynamics, which are run at a sample rate of 1000 Hz. The closed-loop simulation model is run within one Simulink™ instance that is slowed down to a near real-time behavior using simulation pacing. In addition, a second

SimulinkTM instance is used to run the model of the mission computer, which provides the optimization and the Safety Gateway functionalities. The two SimulinkTM instances are used to represent the proposed system concept with an asynchronous calculation and verification of the optimal trajectory. A User Datagram Protocol (UDP) interface is used for the communication between mission computer and FCC in the MIL simulation. Note that this interface must be replaced for an onboard application by a more reliable communication protocol that guarantees delivery and provides error-checking and correction. However, for the purpose of this study, the UDP communication is robust enough and therefore sufficient.

5.2 Comparison between Optimal and Clothoid-based Approach

An exemplary flight plan is used to demonstrate the improvement of the onboard optimization approach compared to the clothoid-based approach (see Section 2 and [3]). Figure 6 shows the waypoints in WGS 84 coordinates that constitute a flight plan with two RF legs. The flight plan starts from WP1 with a straight line segment heading west towards WP2, after which the first 180 deg RF turn with a radius of 2000 m and an exit course angle of 90 deg is to be conducted. Then another straight line segment follows connecting WP3 and WP4. Thereafter, the second 180 deg RF turn follows with a radius of $1600\,\mathrm{m}$ and an exit course angle of $270\,\mathrm{deg}$. The entire flight plan is flown at a constant altitude of 5000 ft above mean sea level, as only the horizontal motion is of interest for the comparison of the optimal and clothoid-based approaches. Initially, the indicated airspeed command is set to 100 KIAS. After reaching WP3, the indicated airspeed command is increased to 118 KIAS so that the second RF turn is flown at a higher speed. All presented results are obtained from simulations without wind and turbulence, as these external effects are compensated by the trajectory controller [4] together with the inner loop and the focus in this study is on the generation of trajectories. The results for the clothoid-based approach were obtained with the same software and simulation settings, the only difference is that the Mission Computer Model on Simulink™ Instance 1 was not executed. By this, optimization requests sent by the FCC were not processed and the clothoid approach is activated as fall-back function by default.

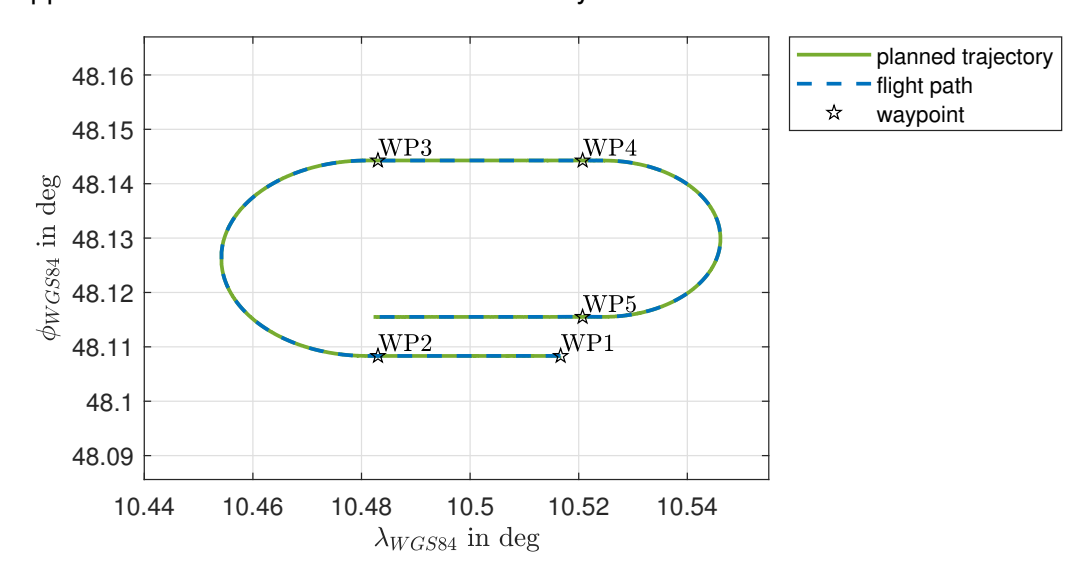


Figure 6 – Simulation results of the flight path and the planned trajectory with optimized RF segments.

The horizontal tracking performance is shown in Figure 7 for both RF legs. The time axis in the plots begins at the moment when WP2 is reached and the first RF turn starts. Dotted vertical lines mark time ranges of turn-entry or turn-exit transitions between straight line and arc segments for which either the optimal or the clothoid-based approach is used. The figure shows the cross track error Δy between the aircraft and the planned trajectory together with its first order derivative $\Delta \dot{y}$. Both variables are inputs to the second order error dynamics trajectory controller and consequently controlled to zero.

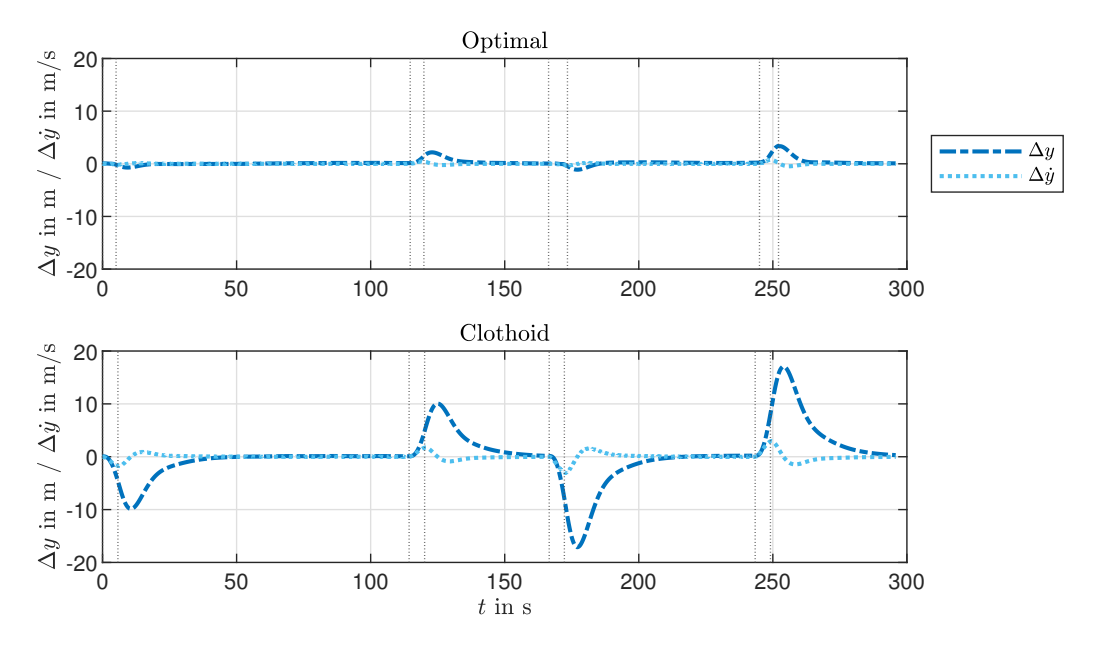


Figure 7 – Horizontal error dynamics for optimal and clothoid approach.

During the turn-entry transition of the first RF leg, a cross track error of $-0.7\,\mathrm{m}$ is built up in case of the optimization approach, which is considerably less than the $-9.9\,\mathrm{m}$ in case of the clothoid-based approach. The decrease in cross track error at the turn entry shows that the optimal approach generates a feed-forward command which improves the ability to keep the aircraft on the planned trajectory. Negative values of the cross track error at the turn-entry indicate that the aircraft is outside the arc of the planned trajectory indicating that the actual roll response of the aircraft is too slow to follow the planned path. At the turn-exit of the first RF leg for the optimization-based solution, the cross track error is $1.5\,\mathrm{m}$ and further increases to $2.2\,\mathrm{m}$ during the first $3\,\mathrm{s}$ of the straight line segment before it declines. With clothoids, a cross track error of $4.9\,\mathrm{m}$ is reached at the end of the transition from arc to straight line, which afterwards increases to $10.1\,\mathrm{m}$ within the first $5\,\mathrm{s}$ of the straight line segment. The positive cross track error at the turn exit means that the aircraft is inside the arc or on the right side (in flight direction) of the straight line segment between WP3 and WP4. This overshoot indicates that the aircraft reacts too slow to reduce the bank angle as required for following the planned trajectory.

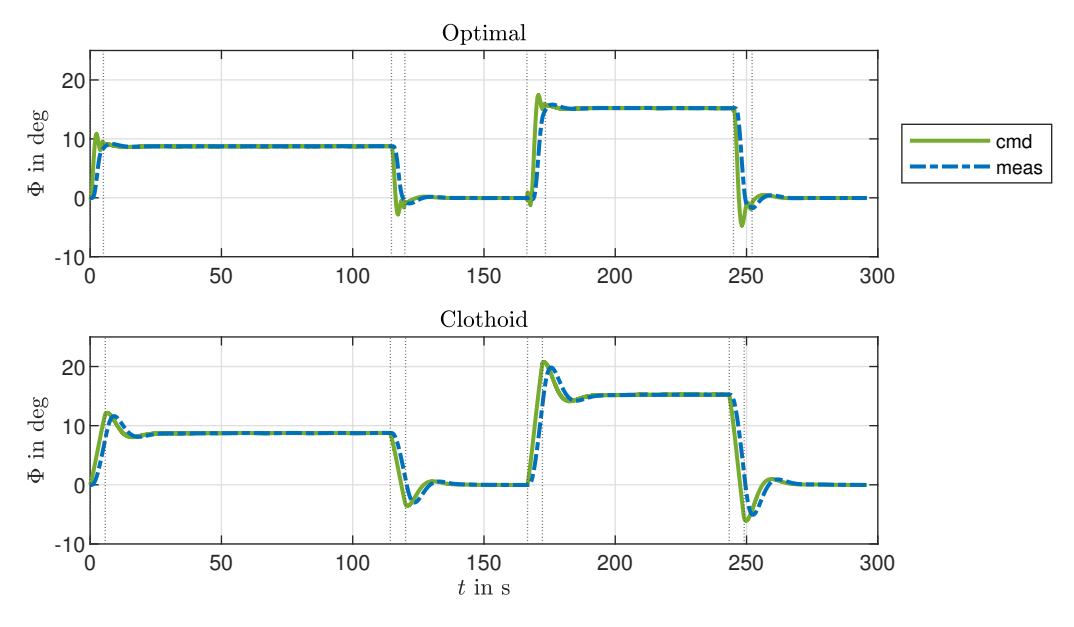


Figure 8 – Bank angle command and aircraft response for optimal and clothoid approach.

The second RF leg requires a higher bank angle due to the smaller turn radius and the higher kinematic speed at which the maneuver is conducted. The improved tracking performance of the optimal approach is again reflected by a smaller cross track error compared to the clothoid approach: At the turn entry, the error increases to $-1.1\,\mathrm{m}$ compared to $-17.1\,\mathrm{m}$ in case of clothoid-based transition. At the turn exit, $3.4\,\mathrm{m}$ are reached at the end of the transition segment and the controller is able to stop a further increase during the straight line segment. In contrast, the clothoid approach results in a further increase of the error to a maximum of $17.1\,\mathrm{m}$ during the straight line segment after exiting the RF turn. Table 1 shows a comparison of the ideal RF circle radius r_P with the radius of the circle segment r_C connecting the turn entry and turn exit transition segments (see Section 2). The differences between r_P and r_C are lower for the optimal trajectory than the clothoid approach. Thus, the optimal approach results in a planned trajectory that is closer to the ideal circle of the RF leg and additionally, the closed-loop controlled aircraft can follow this trajectory with smaller deviations.

Table 1 – Comparison of turn radius for clothoid and optimal approach

	Planned (r_P)	Clothoid (r_c)	Optimal (r_c)
First RF	2000 m	1996.8 m	1998.4 m
Second RF	1600 m	1595.5 m	1597.8 m

Figure 8 compares the Euler roll angle command tracking of the optimal and the clothoid-based approach. The Euler roll angle command, Φ_{cmd} , is generated by the trajectory controller as an input to the inner loop controller. At the beginning of each transition phase, the clothoid approach shows an almost linear change of the roll angle command, which results from the characteristic linear curvature increase of the clothoids. As a consequence of the aircraft's inability to follow this linear roll angle change, the roll angle command further increases due to the additional roll command resulting from the error dynamics to bring the aircraft back on the planned trajectory. This effect explains the overshoot peaks in roll angle command and response at the end of each entry and exit transition. In contrast, the roll angle response in case of the optimal approach shows smooth increases and decreases to stationary values with only minor overshoots of less than $2 \deg$. This roll angle command is defined by the optimization result providing the feed-forward part of the command. It can therefore be shaped to provide desired characteristics.

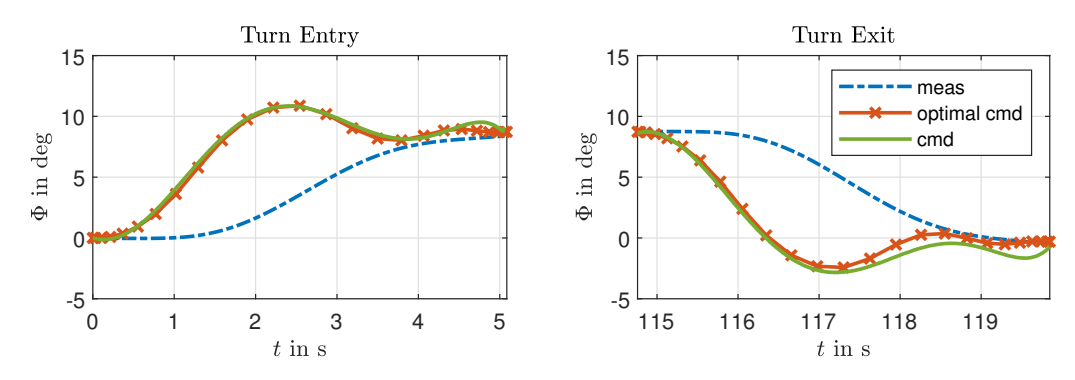


Figure 9 – Euler bank angle command tracking during turn entry and exit transitions of the first RF leg.

Figure 9 provides a detailed view of the roll angle command (*cmd*) that is provided as input to the inner loop and the aircraft's response (*meas*) for the optimal approach during the first RF leg. One can see that the inner loop command (*cmd*) and the output of the optimization for the roll angle command (*optimal cmd*) match almost perfectly for the turn entry. The crosses along the *optimal* signal refer to the collocation points of the optimal command history, which show a higher density at the beginning and end of the turn entry transition to better capture the more dynamic parts of the maneuver and achieve an improved tracking performance in the begin and end of the transition. Considering the turn exit in Figure 9, the command starts to deviate from the optimal solution towards

the end of the transition due to the increasing effect of the error controller, which tackles the emerging cross track error (see also Figure 7). However, the solution is still significantly improved compared to the clothoid-based approach.

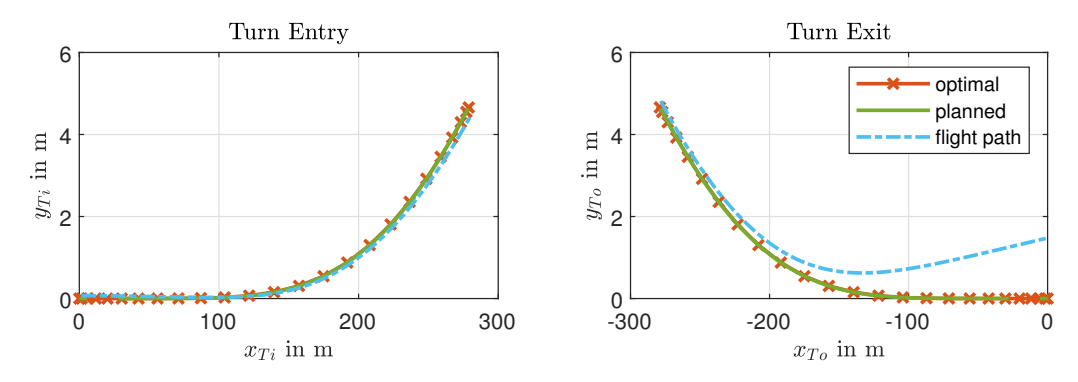


Figure 10 – Comparison of optimal result, planned and flown path of first RF leg.

Figure 10 shows the transition maneuvers for turn entry and turn exit in the horizontal plane of the Ti-frame, or To-frame. Similar to the Ti-frame, which was introduced in Section 3, the To-frame has its origin in the exit fix of the RF leg (WP3) and is derived by rotating the North-East-Down (O) frame by the exit course angle χ_{To} about the z_O -axis such that the x_{To} -axis points along the outbound tangent. Crosses along the path of the optimal solution refer to the distribution of collocation points. One can see that the *planned* trajectory that is generated for the FCC and used for path following control matches the *optimal* solution. The *flight path* shows the actual aircraft position states transformed into the Ti-frame for the turn entry and into the To-frame for the turn exit of the first RF maneuver. In accordance with the negative cross track error shown in Figure 7, one can see that the aircraft is slightly outside of the arc of the *planned* trajectory at the end of the turn entry segment. At the turn exit, Figure 7 shows that the aircraft builds up a positive cross track error of $1.5\,\mathrm{m}$. This cross track error can also be seen in Figure 10 by comparing the *flight path* with the *plannend* trajectory towards $x_{To} = 0\,\mathrm{m}$.

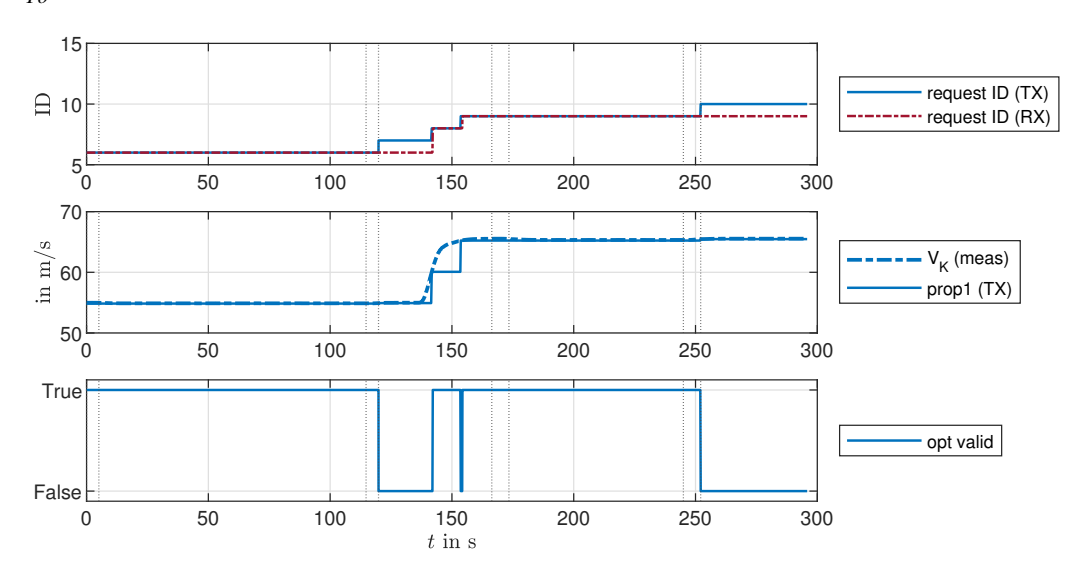


Figure 11 – Data transmitted (TX) or received (RX) by FCC and validity of optimization results.

Finally, the communication between FCC and Mission Computer is analyzed. Figure 11 shows the selected data that was sent or received within the SimulinkTM instance executing the FCC software. For visualization, the data is sampled and hold, i.e., a previous value is hold until a new value is sent or received. The timeline is consistent with the other figures and begins with t = 0s, i.e., when WP2 is reached and the first RF turn starts. Initially, the last sent $Request\ ID$ matches the last received $Request\ ID$, which means that the last received optimization results are stored for usage in the $Trajectory\ Data\ Buffer$ on the FCC. The $opt\ valid$ flag indicates that the received optimization

results passed the Safety Gateway check and are declared as valid by the Monitoring subsystem of the TrajGen function. Directly after the first RF leg, a new optimization request is sent as an upcoming RF maneuver is detected by the change of the NEXT waypoint to WP5, which is another RF type waypoint. When transmitting a new optimization request, the Request ID changes and the opt valid status flag is immediately set to False due to the mismatch of transmitted and received Request IDs. No feasible solution can be calculated by the optimization for the request sent with the ID=7. Therefore no new message is received by the FCC and no new request is triggered as long as the flight and environmental conditions remain unchanged. The middle plot in Figure 11 shows the measured kinematic velocity V_K (meas) and prop1, which refers to a custom field of the last transmitted optimization request. In case of the RF maneuver type, this custom field contains the kinematic velocity that is used as input by the optimization algorithm. Comparing these values shows that a new optimization request is triggered whenever V_K (meas) deviates more than 5 m/s from the kinematic velocity value that is used for the last optimization request. This cyclic re-optimization is triggered by the Monitoring subsystem of the TrajGen function and ensures that the increase in speed as commanded by the operator is taken into account by the optimization. Note that the threshold of 5 m/s is used here only to illustrate the cyclic re-optimization and needs to be adjusted for a real-world application to ensure that the optimization is performed taking into account the latest measured flight conditions. Before the start of the second RF maneuver, valid and feasible optimization results are again available that take into account the latest information on the kinematic speed.

Overall, the proposed optimization-based RF transition maneuver trajectory generation module proved its viability for the application on a CS-23 aircraft. Through the example it became specifically clear that a significantly improved tracking performance can be achieved by the optimization-based approach, which, in turn, results in e.g. reduced fuel consumption and thus extended exploration radius.

6. Conclusion and Future Work

This study introduced an onboard trajectory optimization methodology for RF maneuvers. The goal of the proposed framework was to improve the trajectory tracking capabilities of the aircraft compared to purely geometrical approaches. The goal was achieved by considering the actual aircraft roll dynamics including the inner loop controller by means of a transfer function within the optimization. To avoid compromising the safety of the FCC and enforcing hard real-time requirements on the solution of the OCP, a *Safety Gateway* architecture was used that checked the optimization results for their viability, falling back to geometrical approaches in case a non-viable solution is detected.

Further work comprises the improvement of the trajectory optimization algorithm to work in a faster manner. Here, trigonometric series-based methods as presented in [26, 27] may prove viable. Additionally, the robustness of the optimized trajectory could be improved by e.g. considering wind uncertainties already in the planning [28]. Finally, the effect of using different transfer functions for turn entry and turn exit should be analyzed in future works. The presented simulation results show larger cross-track errors at the turn exit compared to the turn entry, suggesting that the optimization algorithm may be improved for this part. Trajectory tracking during the turn exit may therefore be improved by using a transfer function that is derived from a banked flight state instead of using a transfer function that is derived from a wings-level flight state.

7. Author Contributions

Optimization model and problem formulation: P.P., D.G.; Optimization solver transcription: P.P.; System concept and interface module for online trajectory optimization: D.G.; Software development: D.G. (Simulink™ model), P.P. (C++ code and S-functions); Model-in-the-Loop simulation environment: D.G.; Comparison between optimal and clothoid-based approach: D.G., P.P.; Writing—original draft preparation: D.G., P.P.; Writing—review and editing: P.P., D.G., F.H.; Supervision, resources and project administration: F.H.;

8. Acknowledgments

The authors wish to thank Zoe Mbikayi for his critical review and his input to improve the quality of this paper.

9. Contact Author Email Address

daniel.gierszewski@tum.de

10. Copyright Statement

The authors confirm that they, and/or their company or organization, hold copyright on all of the original material included in this paper. The authors also confirm that they have obtained permission, from the copyright holder of any third party material included in this paper, to publish it as part of their paper. The authors confirm that they give permission, or have obtained permission from the copyright holder of this paper, for the publication and distribution of this paper as part of the ICAS proceedings or as individual off-prints from the proceedings.

References

- [1] International Civil Aviation Organization, *ICAO Doc 9613, Performance-based Navigation (PBN) Manual.* International Civil Aviation Organization, 3 ed., 2008.
- [2] Universal Avionics System Corporation, "Understanding Required Navigation Performance (RNP) and Area Navigation (RNAV) Operations (Doc No.: WHTP-2013-16-10)." https://skybrary.aero/sites/default/files/bookshelf/4108.pdf, 10 2013.
- [3] D. Gierszewski, V. Schneider, P. Lauffs, L. Peter, and F. Holzapfel, "Clothoid-augmented online trajectory generation for radius to fix turns," *IFAC-PapersOnLine*, vol. 51, pp. 174–179, Jan. 2018.
- [4] S. Schatz, Development and Flight-Testing of a Trajectory Controller Employing Full Nonlinear Kinematics. PhD thesis, Technische Universität München, 2018.
- [5] P. Piprek, M. M. Marb, P. Bhardwaj, and F. Holzapfel, "Trajectory/path-following controller based on nonlinear jerk-level error dynamics," *Applied Sciences*, vol. 10, p. 8760, Dec. 2020.
- [6] V. Schneider, P. Piprek, S. P. Schatz, T. Baier, C. Dörhöfer, M. Hochstrasser, A. Gabrys, E. Karlsson, C. Krause, P. J. Lauffs, N. C. Mumm, K. Nürnberger, L. Peter, P. Spiegel, L. Steinert, A. Zollitsch, and F. Holzapfel, "Online trajectory generation using clothoid segments," in 2016 14th International Conference on Control, Automation, Robotics and Vision (ICARCV), pp. 1–6, 2016.
- [7] P. Piprek, V. Schneider, V. Fafard, S. P. Schatz, C. Dörhöfer, P. J. Lauffs, L. Peter, and F. Holzapfel, "Enhanced kinematics calculation for an online trajectory generation module," *Transportation Research Procedia*, vol. 29, p. 312–322, Feb. 2018.
- [8] J. Brandse, M. Mulder, and M. van Paassen, "Advanced trajectory design for the tunnel-in-the-sky display: The use of clothoids," in *AIAA Guidance, Navigation, and Control Conference and Exhibit*, (Reston, Virigina), American Institute of Aeronautics and Astronautics, Aug. 2004.
- [9] P. Mellodge, A Practical Approach to Dynamical Systems for Engineers. Elsevier, 2016.
- [10] A. Steinert, F. Holzapfel, R. Steffensen, and C. Merkl, "Flight test based gain tuning using non-parametric frequency domain methods," in *AIAA Scitech 2021 Forum*, American Institute of Aeronautics and Astronautics, Jan. 2021.
- [11] A. Steinert, R. Steffensen, D. Gierszewski, M. Speckmaier, F. Holzapfel, R. Schmoldt, F. Demmler, U. Schell, M. Ornigg, and M. Koop, "Experimental results of flight test based gain tuning," in AIAA SCITECH 2022 Forum, American Institute of Aeronautics and Astronautics, Jan. 2022.
- [12] M. Rieck, M. Bittner, B. Grüter, J. Diepolder, P. Piprek, C. Göttlicher, F. Schwaiger, B. Hosseini, F. Schweighofer, T. Akman, and F. Holzapfel, "FALCON.m User Guide," 2023.
- [13] A. Wächter and L. T. Biegler, "On the implementation of an interior-point filter line-search algorithm for large-scale nonlinear programming," *Mathematical Programming*, vol. 106, pp. 25–57, Apr. 2005.
- [14] J. Hogg and J. Scott, "HSL_MA97: a bit-compatible multifrontal code for sparse symmetric systems," Nov. 2011. SCD Computational Mathematics Group, RAL-TR-2011-024.
- [15] S. P. Schatz, V. Schneider, E. Karlsson, F. Holzapfel, T. Baier, C. Dörhöfer, M. Hochstrasser, A. Gabrys, C. Krause, P. J. Lauffs, N. C. Mumm, K. Nürnberger, L. Peter, P. Spiegel, L. Steinert, and A. W. Zollitsch, "Flightplan flight tests of an experimental da42 general aviation aircraft," in 2016 14th International Conference on Control, Automation, Robotics and Vision (ICARCV), pp. 1–6, Nov. 2016.

ONBOARD TRAJECTORY OPTIMIZATION FOR RF TURNS

- [16] F. Holzapfel, D. Gierszewski, and M. Speckmaier, "FADEAPC Vollelektronische Triebwerks- und Propellersteuerung für CS-23 Turbopropflugzeuge; Full-authority digital engine and propeller control: Schlussbericht: Förderprogramm: LuFo V-2: Laufzeit des Vorhabens: 01.02.2016-30.06.2022," 2022.
- [17] European Union Aviation Safety Agency (EASA), "Certification Specifications for Normal-Category Aeroplanes (CS-23)," standard, European Union Aviation Safety Agency (EASA), 2020.
- [18] F. Holzapfel, C. Schropp, A. Gabrys, D. Gierszewski, and M. Speckmaier, "Verbundvorhaben HOPLA Hybrid optionally piloted long endurance aircraft; Teilvorhaben: Entwicklung eines hybriden Flugsteuerungssystems mit mechanisch-elektrischer Uebertragung für den Einsatz in einem OPV: LuFo V-1: Schlussbericht," 2019.
- [19] S. P. Scherer, M. Speckmaier, D. Gierszewski, A. Steinert, and F. Holzapfel, "Compensation of nonlinear transmission effects in electro-mechanical flight control systems," in *AIAA SCITECH 2022 Forum*, American Institute of Aeronautics and Astronautics, Jan. 2022.
- [20] D. M. Gierszewski, V. Fafard, F. Schweighofer, P. Piprek, M. Speckmaier, and F. Holzapfel, "Toward on-board trajectory optimization for fuel-saving climb of aircraft with automatic flight control," in *Proceedings of the 2022 CEAS EuroGNC conference*, (Berlin, Germany), May 2022. CEAS-GNC-2022-044.
- [21] C. Krammer, F. Schweighofer, D. Gierszewski, S. Scherer, T. Akman, H. Hong, and F. Holzapfel, "Requirements-based generation of optimal vertical takeoff and landing trajectories for electric aircraft," in 33rd Congress of the International Council of the Aeronautical Sciences (ICAS), Sep. 2022.
- [22] V. Schneider, Trajectory Generation for Integrated Flight Guidance. Verlag Dr. Hut, May 2019.
- [23] Aeronautical Radio, Inc., "ARINC Specification 424-20: Navigation System Database," standard, Aeronautical Radio, Inc., 2011. ARINC 424-20.
- [24] M. Hochstrasser, C. Krause, V. Schneider, and F. Holzapfel, "Model-based implementation of an onboard stanag 4586 vehicle specific module for an air vehicle," in *AIAA Modeling and Simulation Technologies Conference*, American Institute of Aeronautics and Astronautics, Jan. 2017.
- [25] A. W. Zollitsch, S. P. Schatz, N. C. Mumm, and F. Holzapfel, "Model-in-the-loop simulation of experimental flight control software," in *2018 AIAA Modeling and Simulation Technologies Conference*, Jan. 2018.
- [26] H. Hong, P. Piprek, R. J. M. a. Afonso, and F. Holzapfel, "Trigonometric series-based smooth flight trajectory generation," *IEEE Transactions on Aerospace and Electronic Systems*, vol. 57, pp. 721–728, Feb. 2021.
- [27] H. Hong, P. Piprek, S. Hu, and F. Holzapfel, "Transition trajectory generation with time-scaled trigonometric series control parameterization," *Aerospace Systems*, vol. 5, p. 523–530, June 2022.
- [28] P. Piprek, S. Gros, and F. Holzapfel, "Rare event chance-constrained optimal control using polynomial chaos and subset simulation," *Processes*, vol. 7, p. 185, Mar. 2019.